INTENSITY MAPPING OF THE [CII] FINE STRUCTURE LINE DURING THE EPOCH OF REIONIZATION

Yan Gong[1], Asantha Cooray[1], Marta Silva[2], Mario G. Santos[2], James Bock[3,4], Matt Bradford[3,4], Michael Zemcov[3,4]

[1]Department of Physics & Astronomy, University of California, Irvine, CA 92697
[2]CENTRA, Instituto Superior Téecnico, Lisboa 1049-001, Portugal
[3]California Institute of Technology, 1200 E. California Blvd., Pasadena, CA 91125, USA and
[4]Jet Propulsion Laboratory, 4800 Oak Grove Drive, Pasadena, CA 91109, USA

Draft version July 20, 2011

ABSTRACT

The atomic CII fine-structure line is one of the brightest lines in a typical star-forming galaxy spectrum with a luminosity $\sim$ 0.1% to 1% of the bolometric luminosity. It is potentially a reliable tracer of the dense gas distribution at high redshifts and could provide an additional probe to the era of reionization. By taking into account of the spontaneous, stimulated and collisional emission of the CII line, we calculate the spin temperature and the mean intensity as a function of the redshift. When averaged over a cosmologically large volume, we find that the CII emission from ionized carbon in individual galaxies is larger than the signal generated by carbon in the intergalactic medium (IGM). Assuming that the CII luminosity is proportional to the carbon mass in dark matter halos, we also compute the power spectrum of the CII line intensity at various redshifts. In order to avoid the contamination from CO rotational lines at low redshift when targeting a CII survey at high redshifts, we propose the cross-correlation of CII and 21-cm line emission from high redshifts. To explore the detectability of the CII signal from reionization, we also evaluate the expected errors on the CII power spectrum and CII-21 cm cross power spectrum based on the design of the future milimeter surveys. We note that the CII-21 cm cross power spectrum contains interesting features that captures physics during reionization, including the ionized bubble sizes and the mean ionization fraction, which are challenging to measure from 21-cm data alone. We propose an instrumental concept for the reionization CII experiment targeting the frequency range of $\sim$ 200 to 300 GHz with 1, 3 and 10 meter apertures and a bolometric spectrometer array with 64 independent spectral pixels with about 20,000 bolometers

Subject headings: cosmology: theory — diffuse radiation — intergalactic medium — large scale structure of universe

1. INTRODUCTION

Carbon is one of the most abundant elements in the Universe and it is singly ionized (CII) at 11.26 eV, an ionization energy that is less than that of the hydrogen. With a splitting of the fine-structure level at 91 K CII is easily excited resulting in a line emission at 157.7 μm through the $^2P_{3/2} \rightarrow ^2 P_{1/2}$ transition. It is now well established that this line provides a major cooling mechanism for the neutral interstellar medium (ISM) (Dalgarno & McCray 1972; Tielens & Hollenbach 1985; Wolfire et al. 1995; Lehner et al. 2004). It is present in multiple phases of the ISM in the Galaxy Wright et al. (1991) including the most diffuse regions Bock et al. (1993) and the line emission has been detected from the photo dissociation regions (PDRs) of star-forming galaxies (Boselli et al. 2002; De Looze et al. 2011; Nagamine et al. 2006; Stacey et al. 2010) and, in some cases, even in $z > 6$ Sloan quasars (Walter et al. 2009).

The CII line is generally the brightest emission line in star-forming galaxy spectra and contributes to about 0.1% to 1% of the total far-infrared (FIR) luminosity (Crawford et al. 1985; Stacey et al. 1991). Since carbon is naturally produced in stars, CII emission is then expected to be a good tracer of the gas distribution in galaxies. Even if the angular resolution to resolve the CII emission from individual galaxies is not available,

the brightness variations of the CII line intensity can be used to map the underlying distribution of galaxies and dark matter (Basu et al. 2004; Visbal & Loeb 2010; Gong et al. 2011). Thus CII intensity mapping may provide an alternative avenue to probe the era of reionization, including the transition from primordial galaxies with PopIII stars alone to star-formation in subsequent galaxies involving an ISM polluted by metals. Thus CII intensity mapping complements attempts to study reionization with low-frequency radio experiments that probes the 21-cm spin-flip line from neutral hydrogen. While those experiments are sensitive to the neutral gas distribution dominated by the IGM, CII will probe the onset of star formation and metal production in $z \sim 6$ to 8 galaxies.

As the CII emission line is a fine-structure line, we can predict its intensity analytically as a function of redshift by considering the spontaneous, stimulated and collisional emission processes (Suginohara et al. 1999; Basu et al. 2004). This intensity changes the brightness spectrum of the cosmic microwave background (CMB) at the frequency corresponding to the CII line (Basu et al. 2004). In this paper, we focus on the CII flux from individual galaxies where the matter density is high and the collisional emission is the dominant process. As a check on our analytical calculations, we also consider results derived from numerical simulations to establish the CII

intensity. The two approaches are generally consistent. We then consider the measurement of the CII intensity fluctuations resulting from the clustering of the galaxy distribution and sources that are present during and towards the end of reionization at $z \sim 6 - 8$.

Experimentally, there are several challenges that one must overcome before the CII intensity fluctuations from high redshifts can be reliably established. First, higher J transitions of CO from dense molecular gas at lower redshifts contaminate the CII line intensity measurements. In particular, one must account for all of CO(2-1) to CO(13-12) emission lines from individual narrow redshift ranges in the foreground between 0 and 6 when probing CII fluctuations at $z > 6$. To the extent to which a variety of existing predictions on the CO intensity can be trusted (Gong et al. 2011; Lidz et al. 2011; Carilli 2011), we generally find that the contamination is mostly below the level of the CII signal. Extending previous studies (Basu et al. 2004; Visbal & Loeb 2010; Gong et al. 2011; Lidz et al. 2011), we propose the cross-correlation of CII line intensity mapping and 21-cm fluctuations as a way to improve studies related to the epoch of reionization. To evaluate the detectability of the CII signal, we calculate the errors on the CII power spectra and CII-21cm cross correlation, respectively, based on the design of potential (sub-)milimeter surveys for the CII emission. For 21-cm, we consider the first generation experiment LOw Frequency ARray[1] (LOFAR) survey as well as the improvement expected from a second generation experiment like the low-frequency extension to the Square Kilometer Array (SKA).

The paper is organized as follows: in the next section, we derive the formulas to calculate the spin temperature of the CII line in the ISM of galaxies and the IGM. In Section 3, we calculate the mean CII intensity analytically and compare it with results derived from a simulation. We show the CII power spectrum in Section 4. In Section 5, we discuss the low-redshift contamination from CO emission lines for CII intensity mapping at $z > 6$ and in Section 6 we propose a cross-correlation between CII and 21-cm line intensity measurements over the overlapping redshift ranges as a way to both distinguish the CII signal from the CO emission and to improve overall constraints on reionization physics. In Section 7 we outline the experimental parameters of a CII spectral mapping experiment designed to probe $z \sim 6$ to 8 CII intensity fluctuations and discuss the detectability of the CII power spectrum and the CII and 21-cm cross-correlation when combined with LOFAR and SKA. We conclude with a summary of our results in Section 8. Throughout this paper, we assume the flat ΛCDM model with $\Omega_m = 0.27$, $\Omega_b = 0.046$, $\sigma_8 = 0.81$, $n_s = 0.96$ and $h = 0.71$ (Komatsu et al. 2011).

2. THE DERIVATION OF THE SPIN TEMPERATURE OF THE CII EMISSION

The CII line intensity can be generated from carbon present in both the interstellar medium (ISM) of individual galaxies and the diffuse intergalactic medium (IGM) in between galaxies. In the ISM of galaxies, CII is expected to be in thermodynamic equilibrium with resonant scattering emission off of CMB photons and the

collisional emission induced by gas in the galaxy. If the number density of gas particles n_{gas} is greater than a critical value n_{cr}, the collisional excitation and de-excitation rate would exceed that of the radiative (spontaneous and stimulated) processes.

Since the ionization potential of carbon is 11.26 eV, below 13.6 eV of hydrogen ionization, the surrounding gas of CII ions can be either neutral hydrogen or electrons. However, because the critical number density of electrons to trigger collisional excitation n_e^{cr} is less than 100 cm^{-3} while the critical number density of neutral hydrogen for collisional excitation n_H^{cr} is about 10^3 to 10^4 cm^{-3} (Malhotra et al. 2001), the electrons can collide with CII ions more frequently than with HI, especially in ionized gas (Lehner et al. 2004; Suginohara et al. 1999). For simplicity and not losing generality, we assume that the ISM is mostly ionized in individual galaxies. Then the CII line emission would mainly be excited by electrons in the ISM (Suginohara et al. 1999).

On the other hand, in the diffuse IGM in between galaxies CII line emission will be mainly due to radiative processes such as spontaneous emission, stimulated emission due to collisions with CMB photons, and a UV pumping effect similar to the Ly-α coupling for the 21-cm emission (Wouthuysen 1952; Field 1958; Hernandez-Monteagudo et al. 2006). We will focus on the CII emission from the ISM of galaxies first and then consider the signal from the IGM. The latter is found to be negligible.

2.1. *The CII spin temperature in the ISM of galaxies*

In the ISM of galaxies, the ratio of thermal equilibrium population of the upper level $^2P_{3/2}$ and lower level $^2P_{1/2}$ of CII fine structure line can be found by solving the statistical balance equation

$$\frac{n_u}{n_l} = \frac{B_{lu}I_\nu + n_e C_{lu}}{B_{ul}I_\nu + A_{ul} + n_e C_{ul}} \quad (1)$$
$$\equiv \frac{g_u}{g_l} \exp[-T_{\star,ul}/T_{S,ul}].$$

Here $A_{ul} = 2.36 \times 10^{-6}$ s^{-1} is the spontaneous emission Einstein coefficient (Suginohara et al. 1999), B_{ul} and B_{lu} are the stimulated emission and absorption coefficients, respectively, $I_\nu \equiv B[T_{CMB}(z)]$ is the intensity of CMB at ν_{ul}, n_e is the number density of electrons, and C_{lu} and C_{ul} are the excitation and de-excitation collisional rates (in cm^{3}s^{-1}), respectively. Note that the UV pumping effect is neglected here and, as we discuss later, it should not affect the result unless the UV intensity inside the galaxy (I_{UV}^{gal}) is higher than 10^{-15} erg/s/cm^2/Hz/sr, which is about 10^6 times greater than the UV background (Giallongo et al. 1997; Haiman et al. 2000). We note that even if the radiative coupling from UV pumping made a small contribution to the spin temperature it would be in the same direction as the collisional coupling since the UV color temperature follows the gas temperature.

The second line of Eq.1 defines the excitation or spin temperature $T_{S,ul}$ of the CII line. The statistical weights are $g_u = 4$ and $g_l = 2$, and $T_{\star,ul} \equiv h\nu_{ul}/k_B \simeq 91$K is the equivalent temperature of the level transition. The excitation collisional rate C_{lu} can be written as (Spitzer

1978; Osterbrock 1989; Tayal 2008)

$$C_{lu} = \frac{8.629 \times 10^{-6}}{g_l \sqrt{T_k^e}} \gamma_{lu}(T_k^e) \exp\left(\frac{-T_{\star,lu}}{T_k^e}\right), \qquad (2)$$

where T_k^e is kinetic temperature of the electron and γ_{lu} is the effective collision strength, a dimensionless quantity.
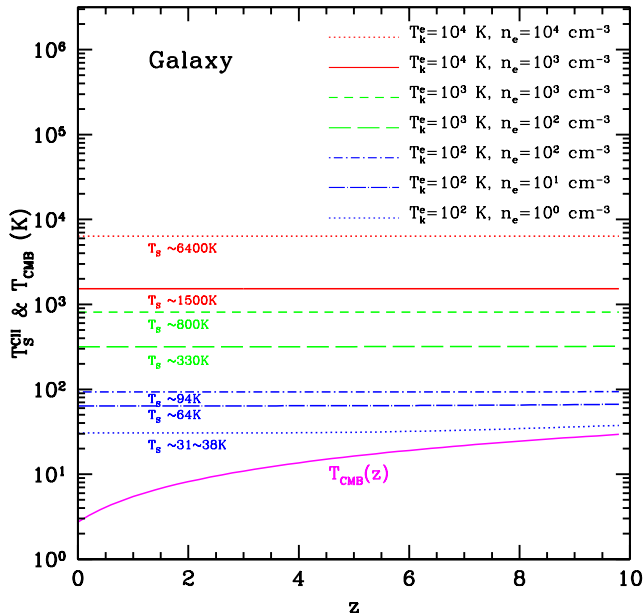

FIG. 1.— The CII spin temperature T_S^{CII} and the T_{CMB} in the ISM of galaxies as a function of the redshift. To capture different ISM conditions within a large sample of galaxies we select several pairs of the electron kinetic temperature T_k^e and the number density n_e for this calculation. We find that the CII spin temperature is almost constant with redshift, which indicates that the collisional process is dominant in the ISM of galaxies when compared to the radiative processes.

To derive the spin temperature T_S, we can use Einstein relations $g_l B_{lu} = g_u B_{ul}$ and $A_{ul} = (2h\nu^3/c^2) B_{ul}$ to convert both stimulated emission coefficient B_{ul} and absorption coefficient B_{lu} in terms of the spontaneous emission coefficient A_{ul}. Also, using the collisional balance relation

$$\frac{C_{lu}}{C_{ul}} = \frac{g_u}{g_l} \exp[-T_{\star,ul}/T_k^e], \qquad (3)$$

we can finally write

$$\frac{T_{\star,ul}}{T_{S,ul}} = log\left\{ \frac{A_{ul}[1 + (I_\nu c^2/2h\nu^3)_{\nu_{ul}}] + n_e C_{ul}}{A_{ul}(I_\nu c^2/2h\nu^3)_{\nu_{ul}} + n_e C_{ul}\exp(-T_{\star,ul}/T_k^e)} \right\}. \qquad (4)$$

Note that the de-excitation collisional rate C_{ul} is dependent on the T_k^e, and using Eq. 2 and Eq. 3, we can calculate the de-excitation collisional rate C_{ul} for a fixed value of the electron kinetic temperature. Here we adopt the values of γ_{lu} which are calculated by the R-matrix in Keenan et al. (1986), and they find $\gamma_{lu} = 1.58$, 1.60 and 2.11 at $T_k^e = 10^2$, 10^3 and 10^4 K respectively. Putting all values together, we find $C_{ul} = 3.41 \times 10^{-7}$, 1.09×10^{-7} and 4.55×10^{-8} cm^{3}s^{-1} for $T_k^e = 10^2$, 10^3 and 10^4 K, respectively. This is well consistent with the de-excitation

rate of 4.6×10^{-8} cm^{3}s^{-1} at 10^4 K given in Basu et al. (2004).

The deviation of the CII spin temperature $T_{S,ul}$ relative to T_{CMB} as a function of redshift for the electron dominated ISM of galaxies is shown in Fig. 1. We choose several values of the electron kinetic temperature T_k^e and the number density n_e to plot the spin temperature T_S as a function of the redshift. We note that although the mean number density of electrons n_e^{mean} can be very small ($< 10^{-2}$ cm^{-3}) in a halo, the significant CII emission in galaxies comes from dense gas clumps which have a much higher n_e (Suginohara et al. 1999). Due to gas clumping the local n_e can be much greater than n_e^{cr} even though $n_e^{mean} < n_e^{cr}$. Thus we choose to assume several high n_e values in our plots, but also show the case with two low values of $n_e = 1$ and 10 cm^{-3}. These values are less than n_e^{cr}. We find the T_S is almost constant and always greater than T_{CMB} for $0 < z < 10$ in all these cases. In Eq. 4, it is easy to find that the T_S depends on the relative strength of the radiative (spontaneous and stimulated) and collisional processes. If the spontaneous and stimulated emission are dominant, we have $T_S \sim T_{CMB}$, while $T_S \sim T_k^e$ if collisions are dominant. Given a fixed number density n_e, the only variable that depends on redshift z in Eq. 4 is $I_\nu(z)$, but the spin temperature is not strongly sensitive to it. This implies that the collisional process is dominant in the ISM of galaxies when compared to the resonant scattering off of CMB photons. As we discuss next, this result is not true for the emission of the CII line in the diffuse IGM (Basu et al. 2004), where T_S is much smaller and varies with redshift similar to T_{CMB}.
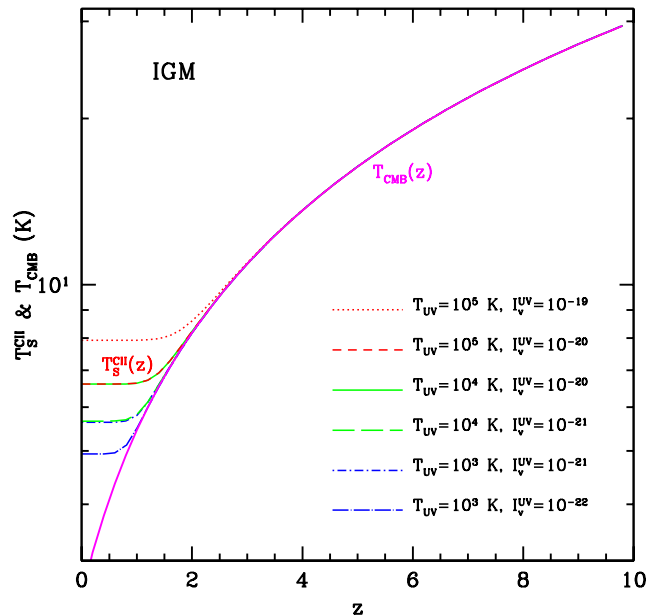

FIG. 2.— The CII spin temperature T_S^{CII} and T_{CMB} in the diffuse IGM as a function of the redshift. We select several pairs of the UV color temperature T_{UV} and the UV background intensity I_ν^{UV} for this calculation. We find the spin temperature is close to T_{CMB} at high redshifts ($z > 2$).

2.2. *The CII spin temperature in the diffuse IGM*

In the IGM, the collisional process becomes unimportant since the number density of electrons and other elements are much smaller than in dense regions within the ISM of galaxies (Basu et al. 2004). Also, the spontaneous emission and the stimulated absorption and emission by the CMB photons are considerable. We will also take into account UV pumping that can enhance CII emission. This effect is similar to the Wouthuysen-Field effect for the 21-cm line (Wouthuysen 1952; Field 1958; Hernandez-Monteagudo et al. 2006) and, to the extent we are aware of, has not been discussed in the literature previously.

At high redshifts the soft UV background at 1330Å generated by the first galaxies and quasars can pump the CII ions from the energy level $2s^2 2p\ ^2P_{1/2}$ to $2s 2p^2\ ^2D_{3/2}$ at 1334.53Å and $2s^2 2p\ ^2P_{3/2}$ to $2s 2p^2\ ^2D_{3/2}$ at 1335.66Å. Then this pumping effect can lead to the CII fine-structure transitions $^2D_{3/2} \rightarrow\ ^2P_{3/2} \rightarrow\ ^2P_{1/2}$, which would mix the levels of the CII line at 157.74μm. The UV de-excitation and excitation rates are given by (Field 1958)

$$P_{\mathrm{ul}}^{\mathrm{UV}} = \frac{g_{\mathrm{k}}}{g_{\mathrm{u}}} \frac{A_{\mathrm{kl}}}{\sum_{\mathrm{n}} A_{\mathrm{kn}}} A_{\mathrm{ku}} \left(\frac{c^2 I_\nu^{\mathrm{UV}}}{2h\nu^3} \right)_{\nu_{\mathrm{ku}}} \qquad (5)$$

and

$$P_{\mathrm{lu}}^{\mathrm{UV}} = \frac{g_{\mathrm{k}}}{g_{\mathrm{l}}} \frac{A_{\mathrm{ku}}}{\sum_{\mathrm{n}} A_{\mathrm{kn}}} A_{\mathrm{kl}} \left(\frac{c^2 I_\nu^{\mathrm{UV}}}{2h\nu^3} \right)_{\nu_{\mathrm{kl}}}, \qquad (6)$$

where "k" stands for the level $^2D_{3/2}$, $g_{\mathrm{k}} = 4$, $A_{\mathrm{kl}} = 2.41 \times 10^8$ s^{-1} and $A_{\mathrm{ku}} = 4.76 \times 10^7$ s^{-1} are the Einstein coefficients of $^2D_{3/2} \rightarrow\ ^2P_{1/2}$ and $^2D_{3/2} \rightarrow\ ^2P_{3/2}$ respectively (see the NIST website [2]), and $\sum_{\mathrm{n}} A_{\mathrm{kn}} = A_{\mathrm{kl}} + A_{\mathrm{ku}}$. Also, it is helpful to define the UV color temperature $T_{\mathrm{UV,ul}}$ in terms of the ratio of the UV de-excitation and excitation rates

$$\frac{P_{\mathrm{lu}}^{\mathrm{UV}}}{P_{\mathrm{ul}}^{\mathrm{UV}}} = \frac{g_{\mathrm{u}}}{g_{\mathrm{l}}} \exp[-T_{\star,\mathrm{ul}}/T_{\mathrm{UV,ul}}]. \qquad (7)$$

Due to the large number of scatterings, the UV color temperature is close to the gas temperature which is easily satisfied in the high-redshift IGM (Furlanetto et al. 2006).

Then, following a similar derivation as to the case of spin temperature in the ISM of galaxies, we find that the CII spin temperature in the diffuse IGM is

$$\frac{T_{\star,\mathrm{ul}}}{T_{S,\mathrm{ul}}} = log\left\{ \frac{A_{\mathrm{ul}}[1 + (I_\nu c^2/2h\nu^3)_{\nu_{\mathrm{ul}}}] + P_{\mathrm{ul}}^{\mathrm{UV}}}{A_{\mathrm{ul}}(I_\nu c^2/2h\nu^3)_{\nu_{\mathrm{ul}}} + P_{\mathrm{ul}}^{\mathrm{UV}}\exp(-T_{\star,\mathrm{ul}}/T_{\mathrm{UV}})} \right\}. \qquad (8)$$

In Fig. 2, we show the departure of T_S from T_{CMB} as a function of the redshift. We see that the T_S^{IGM} does not change if $T_{\mathrm{UV}} > 10^3$ K when fixing I_ν^{UV}, and it is close to T_{CMB} at high redshifts ($z > 2$). Together with Eq. 8 this implies that $A_{\mathrm{ul}} \gg P_{\mathrm{ul}}^{\mathrm{UV}}$, i.e. the spontaneous and stimulated emission are much greater than the UV pumping effect at high redshifts. By comparing Fig. 2 with Fig. 1, we can see that the CII spin temperature in the ISM of galaxies is much larger than that of the

[2] http://physics.nist.gov/PhysRefData/ASD/lines_form.html

diffuse IGM, and T_S^{IGM} is quite close to T_{CMB} at high redshift while T_S^{gal} is larger than T_{CMB}.

3. THE CALCULATION OF THE CII MEAN INTENSITY

To establish the overall intensity of the CII line emission we calculate the distortion of the CMB spectrum ΔI_ν and take into account the mean intensity of the CII line emitted by the ISM galaxies and the IGM. Considering the spontaneous, stimulated emission and absorption, and the expansion of the Universe, we write the radiative transfer equation as

$$\frac{dI_\nu(z)}{ds} = j_\nu(z) - \alpha_\nu(z)I_\nu - 3\frac{H(z)}{c}I_\nu, \qquad (9)$$

where ds is the line element along the line of sight, and $H(z)$ is the Hubble parameter. The spontaneous emission and absorption coefficients are

$$j_\nu(z) = \frac{h\nu_{\mathrm{ul}}}{4\pi} n_{\mathrm{u}}(z) A_{\mathrm{ul}} \phi(\nu)$$

and

$$\alpha_\nu(z) = \frac{h\nu_{\mathrm{ul}}}{4\pi} \phi(\nu)(n_{\mathrm{l}} B_{\mathrm{lu}} - n_{\mathrm{u}} B_{\mathrm{ul}})$$

respectively, where $\phi(\nu)$ is the line profile function which can be set as delta function $\phi(\nu') = \delta(\nu' - \nu)$ if the thermal broadening or velocity is much smaller than the frequency resolution (Suginohara et al. 1999; Basu et al. 2004). Integrating Eq.9 along the line of sight then gives

$$\Delta I_\nu = \int \frac{j_\nu(z) - \alpha_\nu(z)I_\nu}{(1+z)^3} ds \qquad (10)$$

$$= \int \frac{j_\nu(z) - \alpha_\nu(z)I_\nu}{H(z)(1+z)^4} cdz.$$

Using the relation of the line profile and the redshift $\phi(\nu') = \phi[\nu_0(1+z')] = [(1+z)/\nu]\delta(z'-z)$ we can obtain the integrated intensity of the CII emission lines at z as

$$\Delta I_\nu = \frac{hc}{4\pi H(z)(1+z)^3} A_{\mathrm{ul}}\ f_{\mathrm{CII}}^{\mathrm{grd}} n_{\mathrm{CII}}(z) \times \quad (11)$$

$$\frac{g_{\mathrm{u}}}{g_{\mathrm{l}}}\exp(-T_{\star,\mathrm{ul}}/T_{S,\mathrm{ul}})\left[1 - \frac{\exp(T_{\star,\mathrm{ul}}/T_{S,\mathrm{ul}}) - 1}{(2h\nu^3/c^2 I_\nu)_{\nu_{\mathrm{ul}}}} \right],$$

where $f_{\mathrm{CII}}^{\mathrm{grd}}$ is the fraction of CII ions at the ground level $^2P_{1/2}$. If $T_S \gg T_\star(> T_{\mathrm{CMB}})$, which is the usual case in the galaxies, then $\exp(\pm T_{\star,\mathrm{ul}}/T_{S,\mathrm{ul}}) \sim 1$, and we can find

$$\Delta I_\nu = \frac{hc}{4\pi H(z)(1+z)^3} \frac{g_{\mathrm{u}}}{g_{\mathrm{l}}} A_{\mathrm{ul}}\ f_{\mathrm{CII}}^{\mathrm{grd}} n_{\mathrm{CII}}(z). \qquad (12)$$

If T_S is much larger than $T_{\star,\mathrm{ul}}$ (e.g. the cases in galaxies), $f_{\mathrm{CII}}^{\mathrm{grd}} \simeq 1/3$ is a good approximation, and when $T_S \ll T_{\star,\mathrm{ul}}$ we can set $f_{\mathrm{CII}}^{\mathrm{grd}} \simeq 1$ (e.g. the case of the IGM). The $n_{\mathrm{CII}}(z)$ is the number density of the CII ions at z, which has to be carefully estimated for both the galaxy and IGM cases.

To calculate the CII intensity, we now need an estimate of the number density of the CII ions. For the IGM case, it is easy to calculate if we know the metallicity evolution and the average baryonic density as a function of z. However, for the ISM of galaxies, we also have to find the fraction of the CII ions which exceed the critical density

to trigger the dominant collisional emission. In the next section, we will first evaluate the $n_{\rm CII}$ theoretically for both the ISM and IGM cases, and then calculate $n_{\rm CII}$ using data from a simulation and compare it to the analytical result as a check on the consistency. We also provide an order of magnitude estimate on the $z \sim 6$ to 8 CII mean intensity using scaling relations such as those involving star-formation rate and the total far-IR luminosity of galaxies.

3.1. *The analytic estimation*

We start by writing

$$n_{\rm CII}(z) = f_{\rm CII}(z)Z_{\rm C}\bar{n}_{\rm gas}(z),$$

where $Z_{\rm C} = X_{\rm C}Z_{\odot}^{\rm C}$, $Z_{\odot}^{\rm C} = 3.7 \times 10^{-4}$ is the solar carbon abundance (Basu et al. 2004), and we assume $X_{\rm C} = 1$ in the galaxy and $X_{\rm C} = 10^{-2}$ in the IGM (Savaglio 1997; Aguirre & Schaye 2005; Kramer et al. 2010). The $f_{\rm CII}(z) = Z/Z_{\odot}(z)$ is the global metallicity at different redshift, and we use an approximated relation $Z/Z_{\odot}(z) = 10^{-0.5z}$ in our calculation, which assumes the present mean metallicity of the Universe is equal to the solar metallicity (note that this assumption may overestimate the metallicity at low redshifts) and the carbon atoms are totally ionized to be CII.

This relation is consistent with the observational data from the damped Ly-α absorbers (DLAs) metallicity measurements, which covers the redshift range from 0.09 to 3.9 (Kulkarni et al. 2005), and also matches a previous theoretical estimation (Pei et al. 1995, 1999). The $\bar{n}_{\rm gas}(z)$ is the mean number density of the gas, which, for the IGM case, is just the baryon density, $\bar{n}_{\rm b}(z) = 2 \times 10^{-7}(1+z)^3 {\rm cm}^{-3}$. For the ISM of galaxies, we use $\bar{n}_{\rm gas}(z) = f_{\rm gas}^{\rm cr}\bar{n}_b(z)$, where $f_{\rm gas}^{\rm cr}$ is the fraction of the gas that are present in dense environments of the ISM and satisfies $n_{\rm gas} \gtrsim n_{\rm cr}$ (Suginohara et al. 1999). The value of $f_{\rm gas}^{\rm cr}$ depends on the gas clumping within the ISM of galaxies and the Jeans mass (Fukugita & Kawasaki 1994; Suginohara et al. 1999). For simplicity, we just take $f_{\rm gas}^{\rm cr} = 0.3$ as the fraction of gas in the ISM in the dense form and we take this to be the case for all galaxies independent of the redshift (Fukugita & Kawasaki 1994; Suginohara et al. 1999). As is clear, this parameter is the least uncertain of the calculation we present here. Observations with ALMA and other facilities of *Herschel* galaxy samples will eventually narrow down this value. As we are computing the mean intensity expected in a cosmological survey, $\bar{n}_{\rm gas}$ is the number density for galaxies in a large space volume instead of one individual galaxy and thus we can still use $\bar{n}_{\rm b}$ for the ISM of galaxies.

In Fig. 3, we plot an analytical estimate of intensity of CII emission line from the ISM of galaxies as a function of redshift. We select the same pairs of $T_{\rm k}^{\rm e}$ and $n_{\rm e}$ as in the Fig. 1. We see that the intensity is practically independent of the electron number density and the temperature when $n_{\rm e} > 10^2$ cm^{-3} and $T_{\rm k}^{\rm e} > 10^3$ K, e.g., the signal is only seen in emission and is essentially proportional to the CII density (see Eq. 12). Even for $n_{\rm e} = 1$ and 10 cm^{-3} which is less than the $n_{\rm e}^{\rm cr}$, we still find a significant intensity for the CII emission from the ISM of galaxies.
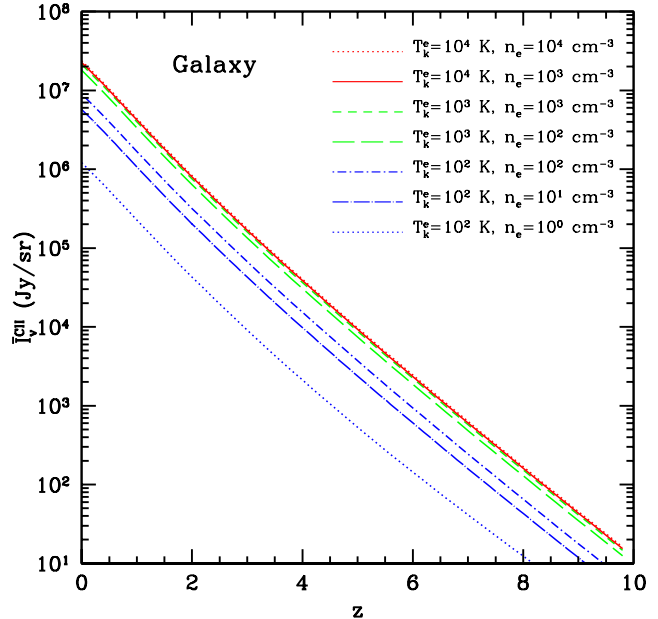

Fig. 3.— The mean intensity of CII emission line from the ISM gas in galaxies as a function of the redshift. We find that the electron collisional emission saturates when $n_{\rm e} \gtrsim 10^2$ cm^{-3} and $T_{\rm k}^{\rm e} \gtrsim 10^3$ K.

In Fig. 4, we show the same for carbon in the diffuse IGM. We find the $I_{\nu}^{\rm CII}$ from the IGM is much smaller than that from galaxies, and $I_{\rm CII}^{\rm gal}/I_{\rm CII}^{\rm IGM} \gtrsim 10^4$ for all cases we consider at all redshifts. This is because the CII spin temperature and the CII abundance in the ISM of galaxies are much larger than that in the diffuse IGM. Thus the CII emission from IGM can be safely neglected,
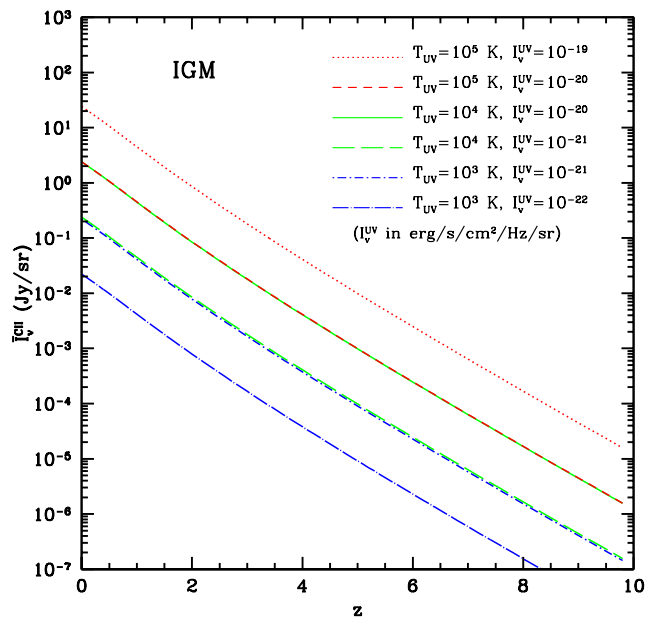

Fig. 4.— The mean intensity of CII emission line from carbon in the IGM as a function of the redshift. The intensity here is much smaller than that of ISM in galaxies since the spin temperature is close to the CMB temperature and the gas density is much lower than galaxy ISM.

and hereafter we will just take into account the CII emission from the ISM of galaxies when discussing intensity fluctuations.

Note the line intensity measurements of individual galaxies are generally described with PDR models using the number density and the UV intensity within the ISM, instead of number density and temperature as we use here (Malhotra et al. 2001). We depart from the PDR modeling approach as we are considering global models that are appropriate for cosmological observations and are not attempting to model the properties of line emission from individual galaxies. It is likely that future work will need to improve our model by making use of a more accurate description of the stellar mass function and the star-formation history of each of the galaxies in a large cosmological simulation by performing calculations to determine T_e given the UV intensity field dominated by the massive, bright stars. When making predictions related to the CII intensity power spectrum (Section 4), we take as default values $T_e = 1000$K and $n_e = 100$ cm^{-3}. These values are fully consistent with the findings of Malhotra et al. (2001), where they find for 60 normal star-forming galaxies, the values of $T \sim 225$ to 1400K and $n \sim 10^2$ to 10^4 cm^{-3}.

3.2. Intensity estimated from numerical simulations

Since the evolution of the metallicity and the critical fraction of the gas f_{gas}^{cr} are hard to estimate, the number density of the CII ions n_{CII} is not well determined analytically for the case involving CII emission from the ISM of galaxies. So we use results derived from a numerical simulation to check the analytical estimation. To do this we first derive the expected CII mass, M_{CII}, in a halo with mass M at a given redshift. Then, by integrating over all possible halo masses in a given volume, we estimate the CII mass for that same volume.
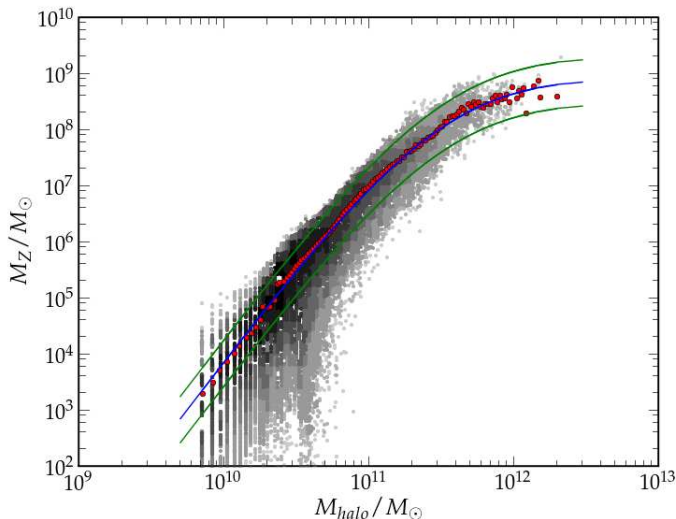

FIG. 5.— The mass in metals M_Z as a function of the halo mass M at z=8. The solid lines shows the mean relation (blue center line) and $\pm 1\sigma$ relation (green lines). The red dots denote the mean value of the scattering (gray region) when binned to 150 logarithmic intervals in halo mass.

To find $M_{CII}(z)$ with simulations, we make use of the

galaxy catalog from De Lucia & Blaizot (2007). This catalog is obtained by post-processing the Millennium dark matter simulation with semi-analytical models of galaxy formation (Springel et al. 2005), and has the metal content in each of four different components: stars, cold gas, hot gas and an ejected component. In this calculation we will assume that the CII emission comes from the hot gas component which has a temperature of about 10^5 - 10^7 K. However, according to Obreschkow et al. (2009a), some of the gas in galactic disks which is considered as cold gas (T $\approx 10^2 - 10^3$ K) in the De Lucia catalog, should actually be warm (T $\approx 10^4$ K) and ionized. So we will also consider the case where 10% of this cold gas from the De Lucia & Blaizot (2007) simulation is recategorized as warm and thus contribute to the CII luminosity.

In Fig. 5 we plot the mass in metals M_Z as a function of the halo mass M for the hot gas only case. There is some scatter, specially at the low mass end, but note that if the experimental volume is large enough, we will be observing a large number density of galaxies such that the total M_Z should approach the average. The average relation between M_Z and halo mass M can be parameterized in the form $M_Z(M) = M_0(M/M_c)^b(1 + M/M_c)^{-d}$. At $z = 6$, $z = 7$ and $z = 8$, these parameters take the values $M_0 = 1.1 \times 10^9$, 1.0×10^9 and 1.6×10^9, $M_c = 3.5 \times 10^{11}$, 3.5×10^{11} and 3.7×10^{11}, $b = 3.6$, 3.4 and 3.4, and $d = 3.25$, 3.1 and 3.6, respectively.

At high ISM temperatures with $T > 100$K we assume carbon is ionized, so we have $M_{CII} = f_\odot^C M_Z$ where $f_\odot^C = 0.21$ is the carbon fraction of the mass in metals in the Sun (Arnett 1996). By taking into account the expected number of halos, we can obtain n_{CII} as

$$n_{CII}^{sim}(z) = \int_{M_{min}}^{M_{max}} dM \frac{dn}{dM} \frac{M_{CII}(M, z)}{m_c}, \qquad (13)$$

where m_c is the atomic carbon mass, M is the halo mass and dn/dM is the halo mass function (Sheth & Tormen 1999). The integration is made from $M_{min} = 10^8$ M$_\odot$/h to $M_{max} = 10^{13}$ M$_\odot$/h, and M_{min} is the minimum mass of the dark matter halo that can host galaxies. From the previous section we can safely assume that the spin temperature is saturated (e.g. the CII is only seen in emission) so that we now have all the ingredients to calculate the signal using the simulation values.

In Fig. 6, we show the number density of the CII ions $n_{CII}^{sim}(z)$ using the simulation result. We find our analytic result is well consistent with that derived from the simulation especially at high redshift. The departure at low redshift in our analytical calculation is reasonable since the metallicity in our analytic approximation may be overestimated at the low redshift end (Kulkarni et al. 2005). Assuming only the hot gas component of De Lucia & Blaizot (2007) contribute to the CII line luminosity, L_{CII}, our two calculational methods differ by a factor of a few; however, after adding the warm component, the analytical result of the previous section match the numerical values at $z > 6$ where we are especially interested. The difference is again same for the mean intensity of the CII emission shown in Fig. 7. Again, we find that the CII emission is saturates when $n_e \gtrsim 10^2$ cm^{-3} and $T_k^e \gtrsim 10^3$ K. For higher values, CII intensity is almost independent of n_e and T_k^e.
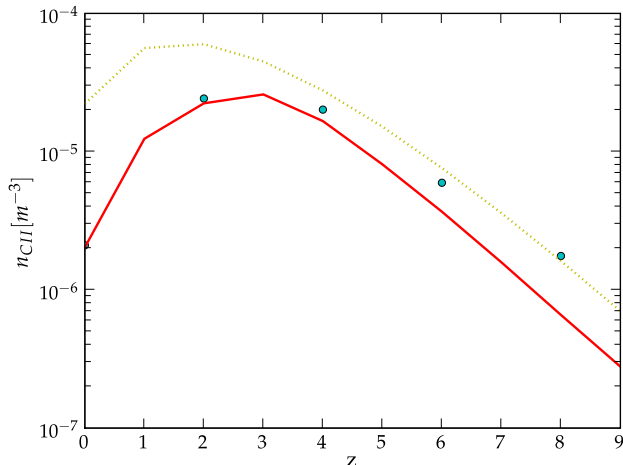
FIG. 6.— The CII proper number density as a function of redshift. The red solid line is derived from our simulation with just hot gas contributing to $L_{\rm CII}$, the yellow dotted line is our analytic result, and the blue spots are obtained from the simulation using both the hot gas and the warm gas (10% of the cold gas in the galaxies; see text for details).
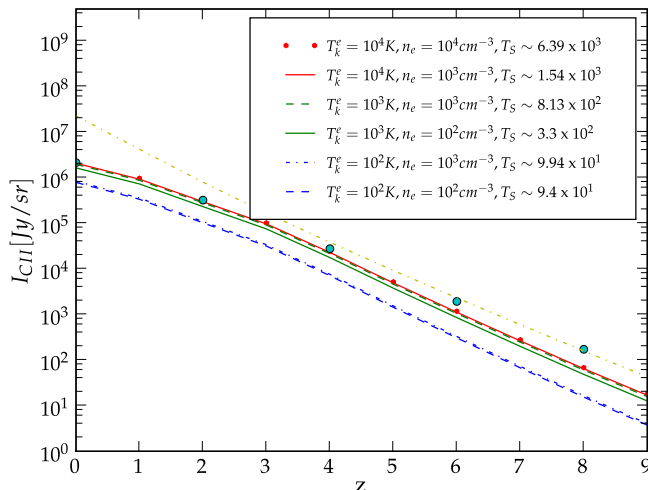

FIG. 7.— The mean intensity of CII emission line from the outputs obtained from the De Lucia & Blaizot (2007) simulation at several different redshifts. The yellow dotted line is our analytic result, and the blue spots are obtained from the simulation with the hot and warm gas contributing to the $L_{\rm CII}$. The yellow line and the blue spot were calculated with $n_{\rm e} = 10^3$ cm^{-3} and $T_{\rm k}^{\rm e} = 10^4$ K. The other lines are derived from the simulation assuming only the hot gas contributes to the $L_{\rm CII}$.

3.3. Intensity estimated from observed scaling relations

At $z \sim 7$, our calculations involving either analytical or through De Lucia & Blaizot (2007) simulations suggest a mean intensity of about 100 to 500 Jy/sr with a preferred value around 200 Jy/sr. We can use an approach based on observed scaling relations, similar to the approach used by Carilli (2011) to estimate the mean CO(1-0) intensity during reionization, to estimate the mean CII intensity. We begin with the star-formation rate from $z \sim 6$ to 8. While estimates exist in the literature from Lyman break galaxy (LBG) dropouts (Bouwens et al.

2008), such estimates only allow a lower estimate of the star-formation rate as the luminosity functions are limited to the bright-end of galaxies and the slope at the low-end is largely unknown and could be steeper than indicated by existing measurements. An independent estimate of the star-formation rate during reionization involve the use of gamma-ray bursts (Kistler et al. 2009). Together, LBG and GBR star-formation rates lead to a range of 0.01 to 0.1 M$_\odot$ yr^{-1} Mpc^{-3} at $z \sim 7$.

We can convert this SFR to the CII luminosity of $\sim 3 \times 10^{40}$ to $\sim 3 \times 10^{41}$ ergs s^{-1} using the observed scaling relation of De Looze et al. (2011) for low-redshift galaxies when averaging over 100 Mpc^3 volumes. We also get a result consistent with this estimate when converting the SFR to total integrated FIR luminosity and then assuming that 10^{-2} to 10^{-3} of the $L_{\rm FIR}$ appears in CII Stacey et al. (2010), again consistent with $z \sim 2$ redshift galaxy samples. Once again we note that our estimate is uncertain if either the SFR to CII luminosity calibration evolves with redshift or the CII to FIR luminosity ratio evolves with redshift. The above range with an order of magnitude uncertainty in the SFR, and subject to uncertain evolution in observed scaling relations from $z \sim 2$ to 7, corresponds to an intensity of 40 to 400 Jy/sr at $z \sim 7$. This range is consistent with our independent estimate, but could be improved in the near future with CII and continuum measurements of high redshift galaxy samples with ALMA.

4. THE CII INTENSITY POWER SPECTRUM

The CII intensity we have calculated is just the mean intensity, so in this Section we will discuss spatial variations in the intensity and consider the power spectrum of the CII emission line as a measure of it. This power spectrum captures the underlying matter distribution and if CII line intensity fluctuations can be mapped at $z > 6$, the line intensity power spectrum can be used to probe the spatial distribution of galaxies present during reionization.

Since the CII emission from the ISM of galaxies will naturally trace the underlying cosmic matter density field, we can write the CII line intensity fluctuations due to galaxy clustering as

$$\delta I_\nu^{\rm CII} = \bar{b}_{\rm CII} \bar{I}_\nu^{\rm CII} \delta(\mathbf{x}), \qquad (14)$$

where $\bar{I}_\nu^{\rm CII}$ is the mean intensity of the CII emission line from the last section, $\delta(\mathbf{x})$ is the matter over-density at the location $\mathbf{x}$, and $\bar{b}_{\rm CII}$ is the average galaxy bias weighted by CII luminosity (see e.g. Gong et al. 2011).

Following Eq. 13 and taking into account that the fluctuations in the halo number density will be a biased tracer of the dark matter, the average bias can be written as (Visbal & Loeb 2010)

$$\bar{b}_{\rm CII}(z) = \frac{\int_{M_{\rm min}}^{M_{\rm max}} dM \frac{dn}{dM} M_{\rm CII}(M) b(z, M)}{\int_{M_{\rm min}}^{M_{\rm max}} dM \frac{dn}{dM} M_{\rm CII}(M)}, \qquad (15)$$

where $b(z, M)$ is the halo bias and dn/dM is the halo mass function (Sheth & Tormen 1999). We take $M_{\rm min} = 10^8$ M$_\odot$/h and $M_{\rm max} = 10^{13}$ M$_\odot$/h. Then we can obtain the clustering power spectrum of the CII emission line

$$P_{\rm CII}^{\rm clus}(z, k) = \bar{b}_{\rm CII}^2 \bar{I}_{\rm CII}^2 P_{\delta\delta}(z, k), \qquad (16)$$

where $P_{\delta\delta}(z,k)$ is the matter power spectrum.

The shot-noise power spectrum, due to discretization of the galaxies, is also considered here. It can be written as (Gong et al. 2011)

$$P_{\mathrm{CII}}^{\mathrm{shot}}(z) = \int_{M_{\mathrm{min}}}^{M_{\mathrm{max}}} dM \frac{dn}{dM} \left(\frac{L_{\mathrm{CII}}}{4\pi D_{\mathrm{L}}^2} y(z) D_{\mathrm{A}}^2 \right)^2, \quad (17)$$

where D_{L} is the luminosity distance, D_{A} is the comoving angular diameter distance and $y(z) = d\chi/d\nu = \lambda_{\mathrm{CII}}(1+z)^2/H(z)$, where χ is the comoving distance, ν is the observed frequency, λ_{CII} is the rest frame wavelength of the CII line. The L_{CII} is the CII luminosity which can be derived from the I_ν^{CII}, and we assume $L_{\mathrm{CII}}(M,z) = B \times M_Z(M,z) \, [L_\odot]$ and finally find $B = 10^{0.63}, 10^{0.36}$, and $10^{0.17}$ at $z = 6, 7$, and 8 respectively. The total CII power spectrum is $P_{\mathrm{CII}}^{\mathrm{tot}}(z,k) = P_{\mathrm{CII}}^{\mathrm{clus}}(z,k) + P_{\mathrm{CII}}^{\mathrm{shot}}(z)$.

In Fig. 8, as an example we plot the clustering, shot-noise and total power spectrum of the CII emission at $z = 6$, $z = 7$ and $z = 8$. Using the `Halofit` code (Smith et al. 2003), we calculate the non-linear matter power spectrum. In order to calculate the intensity of the CII line we use $T_{\mathrm{k}}^{\mathrm{e}} = 10^3$ K and $n_{\mathrm{e}} = 10^2 \, \mathrm{cm}^{-3}$, which are a possible representation of the conditions at which CII emits in the galaxies (Malhotra et al. 2001). For comparison, the CII power spectrum estimated by other works are also shown here. The blue dash-dotted line denotes the $P_{\mathrm{CII}}^{\mathrm{tot}}$ derived from the relation $L_{\mathrm{CII}}/L_{\mathrm{CO(1-0)}} \simeq 10^4$ (Breuck et al. 2011), and the $L_{\mathrm{CO(1-0)}}$ is from the calculation of Visbal & Loeb (2010). The magenta long dashed line is the $P_{\mathrm{CII}}^{\mathrm{tot}}$ evaluated via the CII luminosity derived by Visbal & Loeb (2010).

As expected the CII power spectrum is larger than the CO(1-0) power spectrum calculated in Gong et al. (2011). Note that the CO intensities predicted by Gong et al. (2011) should be corrected by a factor of $1/(1+z)$ which comes from a missing conversion factor between the CO flux obtained from Obreschkow et al. (2009b) and the actual CO(1-0) luminosity. Although this correction further reduces the CO signal, we point out that the model we assumed for the CO luminosity as a function of the halo mass generates a steep dependence at the low mass end. If we use a less steep model at the low end of halo masses ($M < 10^{10}$ $\mathrm{M}_\odot$/h), where the simulation has a large scatter, such as $L_{\mathrm{CO(1-0)}} \propto M_{\mathrm{halo}}$, then the CO signal can increase by a factor of a few, partially compensating the $1/(1+z)$ correction.

Comparing the CO(1-0) power spectrum (using the $1/(1+z)$ correction but keeping the luminosity model used in Gong et al. (2011)) with the CII one with its density estimated using only the hot gas component from the simulation, implies a luminosity relation of $L_{\mathrm{CII}}/L_{\mathrm{CO(1-0)}} \approx 4 \times 10^4$ when $z \sim 6$ reducing to below 10^4 when $z \sim 8$. The observational value for this relation as valid for $0 < z < 2$ is $L_{\mathrm{CII}}/L_{\mathrm{CO(1-0)}} = 4100$ as obtained by Stacey et al. (1991) (see also Stacey et al. 2010). However detections of CII emission from star-forming galaxies at $z > 6$ is almost non-existent and there is a strong possibility for an evolution with redshift for this relation. For the handful of galaxies studied, the possibility for evolution is supported by the $L_{\mathrm{CII}}/L_{\mathrm{CO(1-0)}} \simeq 10^4$ value derived for LESS J033229.4-275619 at $z = 4.76$ (Breuck et al. 2011), which is one of the highest redshift CII detections in a sub-mm selected, star-formation dominated galaxy by far, though higher redshift detections are soon expected as part of *Herschel* followup campaigns. In Fig. 8 we show that this observational ratio (blue dash-dotted line) is consistent with our direct CII prediction from the simulation with the hot gas case (red solid line) around 1σ level (green dashed lines, calculated using the 1σ error of the M_Z-M relation). The noise power spectrum and the error bars are estimated for an assumed (sub-)milimeter survey, which we will discuss in some detail in Section 7.

The luminosity formula in Visbal & Loeb (2010) based on the observed sub-mm and mm emission line ratios (see below for CO version) can also be used to calculate the the CII power spectrum as a function of the redshift, but it leads to a result (long dashed magenta line) that is smaller than that estimated by the L_{CII}-$L_{\mathrm{CO(1-0)}}$ relation (blue dash-dotted line). This is effectively due to a difference in the calibration with CO(1-0) luminosity from M82 and CII luminosity from a sample of low redshift galaxies.

In Fig. 9, we plot the intensity maps of the CII emission at $z = 6$, 7 and 8 using De Lucia & Blaizot (2007) simulations to calculate the CII line intensities to show what the sky looks like at each of these redshifts when mapped with CII. The emission can be traced to individual galaxies. Each of these maps span 3 degrees in each direction and the color bar to the right show the intensity scaling in units of Jy/sr. Note the large reduction in the maximum intensity from $z = 6$ to $z = 8$ due to the decrease in the overall abundance of metal content in the ISM of galaxies at high redshifts.

5. CO CONTAMINATION TO CII LINE INTENSITY VARIATIONS

When attempting to observe the $z > 6$ CII line intensity variations, the same observations will become sensitive to variations in the intensity of other emission lines along the line of sight. In particular low-redshift variations will be imprinted by a variety of CO transitions. This foreground line contamination distorts the CII signal and introduces additional corrections to the measured power spectrum, which will not be due to CII alone.

As an example here we will focus on the contamination from the CO lines as we expect those intensities to be of the same order of magnitude as the CII line intensity. Given the difference in the CII rest frequency and those of the CO spectrum for each of the transitions, for a given redshift targeting CII line emission, the frequency of observations and the bandwidth of the observations will correspond to a certain low redshift range in which contaminating CO contribution will be present. Here we calculate the CO power spectrum following Visbal & Loeb (2010) with a CO luminosity formula as the function of the redshift and halo mass (Visbal & Loeb 2010)

$$L_{\mathrm{CO(m-n)}} = 6.6 \times 10^6 \left(\frac{R_{\mathrm{line}}}{3.8 \times 10^6} \right) \left(\frac{M}{10^{10} M_\odot} \right) \quad (18)$$

$$\times \left(\frac{1+z}{7} \right)^{3/2} \frac{f_*}{\epsilon_{\mathrm{duty}}} L_\odot,$$

where R_{line} is the ratio of star formation rate and the luminosity for a emission line, $f_* = 0.1$ is the fraction
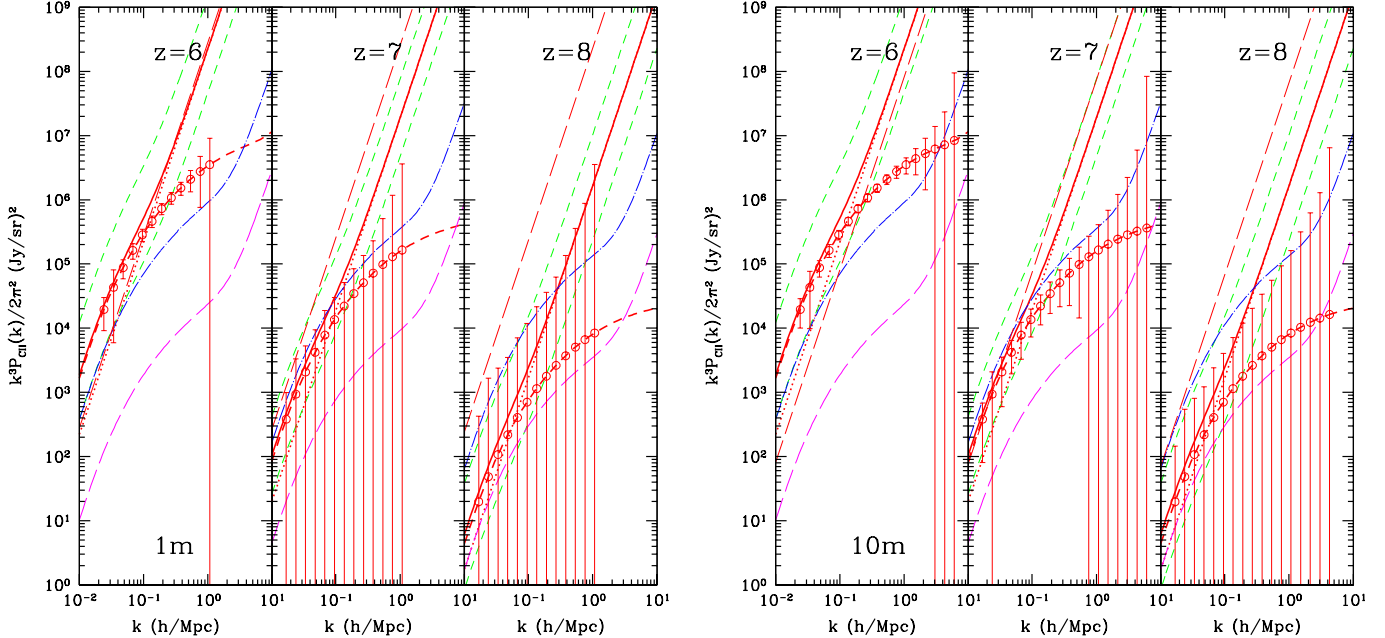
FIG. 8.— The clustering, shot-noise and total power spectrum of CII emission line at $z = 6$, $z = 7$ and $z = 8$. The red solid, dashed and dotted lines denote the CII total, clustering and shot-noise power spectrum respectively. The $P_{\mathrm{CII}}^{\mathrm{clus}}$ is estimated from the simulation with only the hot gas contributing to L_{CII}, and we assuming that $T_{\mathrm{k}}^{\mathrm{e}} = 10^3$ K and $n_{\mathrm{e}} = 10^2$ cm^{-3} here. The green dashed lines are the 1σ error of the CII power spectrum which are derived from the 1σ error of $M_z - M$ relation in Fig. 5. The error bars and noise power spectrum (red long-dashed line) in the left and right panels are estimated with 1m and 10m aperture for CII line respectively. The magenta long dashed line is derived from the CII luminosity estimated by Visbal & Loeb (2010). The blue dash-dotted line is estimated via the relation $L_{\mathrm{CII}}/L_{\mathrm{CO}(1-0)} \simeq 10^4$.

of gas in a halo that can form stars, and $\epsilon_{\mathrm{duty}} = 0.1$ is the duty cycle which is canceled when computing the CO intensity in Visbal & Loeb (2010).

We find this formula has some deviations from the results of our previous simulations (Gong et al. 2011), but it is still a good approximation when considering the halo mass range $10^8 < M < 10^{13}$ M$_\odot$/h in which we perform the calculation. The advantage of this formula is that we can calculate the luminosity of the CO lines at an arbitrary halo mass and redshift. Also, note that take assume $L_{\mathrm{CO}} \sim M$ instead of $L_{\mathrm{CO}} \sim M_{\mathrm{CO}}$ when calculating the large-scale structure bias factor of CO emitting galaxies.

We show how the CO contamination for CII intensity measurements from a variety of redshift ranges for $J = 2-1$ to $J = 13-12$ transitions of CO combine in Fig. 10. The frequency of the CII line which is emitted at high redshift, e.g. $z = 7$, will be redshifted to $\nu_0 = \nu_{\mathrm{CII}}/(1 + z) \simeq 237$ GHz at present. As shown in Fig. 10 the main contamination is from the first five CO lines, CO(2-1) to CO(6-5), and the contamination of the CO lines provide about 2% and 30% to the total intensity power spectrum at $z = 7$ and $z = 8$, respectively, for large scales ($k < 1$ h/Mpc). The black solid lines shown in the plot are the contaminated CII total power spectrum for the hot gas case of our simulation, which is the sum of the CII total power spectrum $P_{\mathrm{CII}}^{\mathrm{tot}}(k)$ (red solid line) and the CO total power spectrum $P_{\mathrm{CO}}^{\mathrm{tot}}(k)$ (dashed and dotted lines). At $z = 6$, the CO contamination is negligible with a correction at the level of 0.1% of the CII signal, while at $z = 8$ CO contamination is ~ 10At small scales ($k > 1$ h/Mpc), the shot noise becomes the dominant

component in the power spectrum, and we find the shot noise of the CII emission is generally greater than that of the CO emission.

6. CROSS-CORRELATION STUDIES BETWEEN CII AND 21-CM OBSERVATIONS

Since the above described CO contamination lines come from different redshifts it is necessary that any CII mapping experiment be considered with another tracer of the same high redshift universe. In particular, low-frequency radio interferometers now target the $z > 6$ universe by probing the neutral hydrogen distribution via the 21-cm spin-flip transition. Thus, we consider the cross correlation of the CII line and the 21-cm emission at the same redshift to eliminate the low-redshift contamination, foregrounds, and to obtain a combined probe of the high redshift universe with two techniques that complement each other. We expect a strong correlation between the CII and 21-cm lines because they both trace the same underlying density field and such a cross-correlation will be insensitive to CO lines since they are from different redshift which depart far away from each other. There could still be lower order effects, such as due to radio foregrounds. For example, the same galaxies that are bright in CO could also harbour AGNs that are bright in radio and be present as residual point sources in the 21 cm data. Then the cross-correlation will contain the joint signal related to low redshift CO emission and the residual point source radio flux from 21-cm observations. The issue of foregrounds and foreground removal for both CII alone and joint CII and 21-cm studies are beyond the scope of this paper. We plan to return to such a topic in an upcoming paper (Silva et
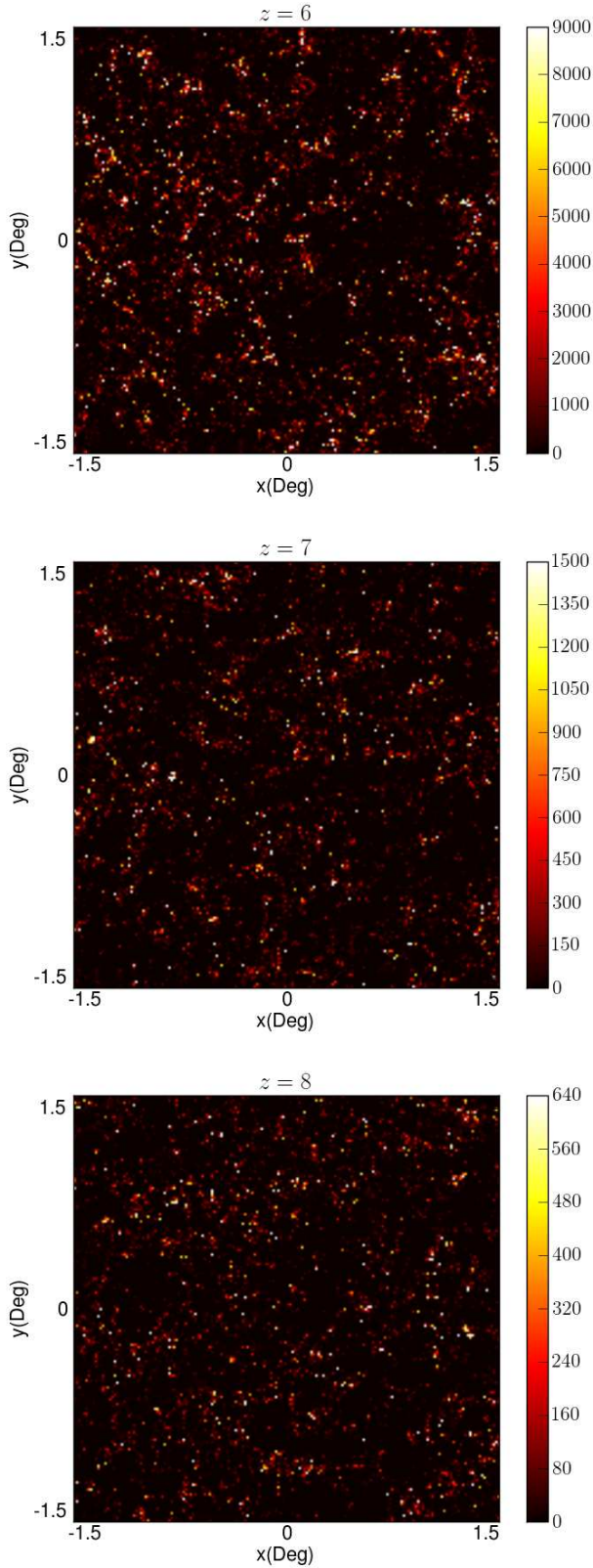
FIG. 9.— The sky maps of the CII emission at $z = 6$, 7 and 8 from top to bottom, respectively using De Lucia & Blaizot (2007) simulations to calculate the CII line intensities. Each of these maps span 3 degrees in each direction and the color bar to the right show the intensity scaling in units of Jy/sr.
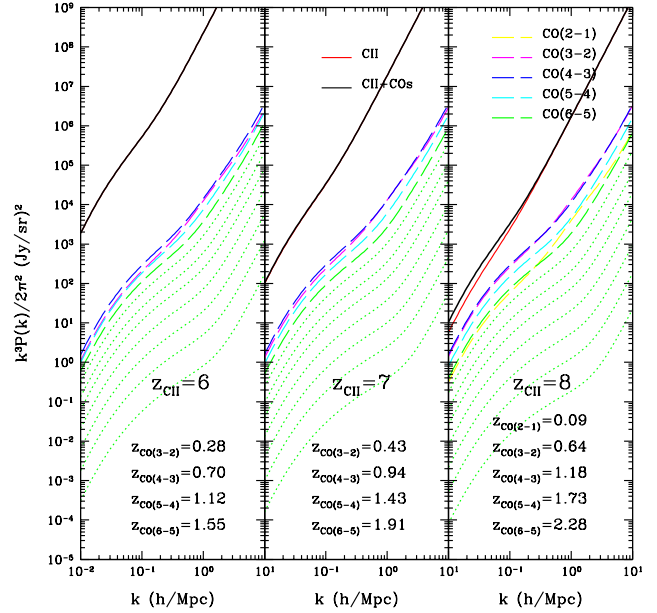

FIG. 10.— The contaminated CII total power spectrum $P_{\rm CII}^{\rm cont}$ (black solid lines) at $z = 6$, $z = 7$ and $z = 8$. The CII total power spectrum $P_{\rm CII}^{\rm tot}$ is calculated from the hot gas in the simulation (red solid line) (note that the $P_{\rm CII}^{\rm cont}$ and $P_{\rm CII}^{\rm tot}$ are almost overlapped at $z = 6$ and $z = 7$ because of the relatively smaller CO line contamination). The other long dashed and green dotted lines are calculated with the $L_{\rm CO(m-n)}$ given in Visbal & Loeb (2010). The green dotted lines from upper to lower are CO(7-6), CO(8-7) ... CO(13-12) respectively.

al. in preparation).

Here we calculate the power spectra for the CII-21cm correlation using the correlation between the matter density field and the 21cm brightness temperature obtained from a simulation made using the Simfast21 code (Santos et al. 2010), with the further modifications described in (Santos et al. 2011) to take into account the unresolved halos. This code uses a semi-numerical scheme in order to simulate the 21cm signal from the Reionization Epoch. The simulation generated has boxes with a resolution of 1800^3 cells and a size of L=1Gpc. With an ionizing efficiency of 6.5 we have obtained the mean neutral fraction fraction of 0.05, 0.35, and 0.62 and an average brightness temperature of 0.63 mK, 6.44 mK, and 14.41 mK for $z = 6$, $z = 7$, and $z = 8$ respectively. The power spectrum of 21-cm emission is also shown in Fig. 11, the blue dashed error bars are estimated from the LOFAR and the red solid ones are from the SKA (see Table 2 for experimental parameters).

In Fig. 12, we show the cross power spectrum of the CII and 21-cm emission line (red thick lines) and 1σ uncertainty (red thin lines) at $z = 6$, $z = 7$ and $z = 8$. The error bars of the cross power spectrum are obtained by the assumed milimeter spectrometeric survey with 1 m and 10m aperture for CII line and LOFAR (left panel) and SKA (right panel) for 21-cm emission. Note that the correlation is negative on large scales (small k) when the correlation between the ionization fraction and the matter density dominates and positive on small scales when the matter density auto-correlation is dominating. This can be seen by looking at the expression for the
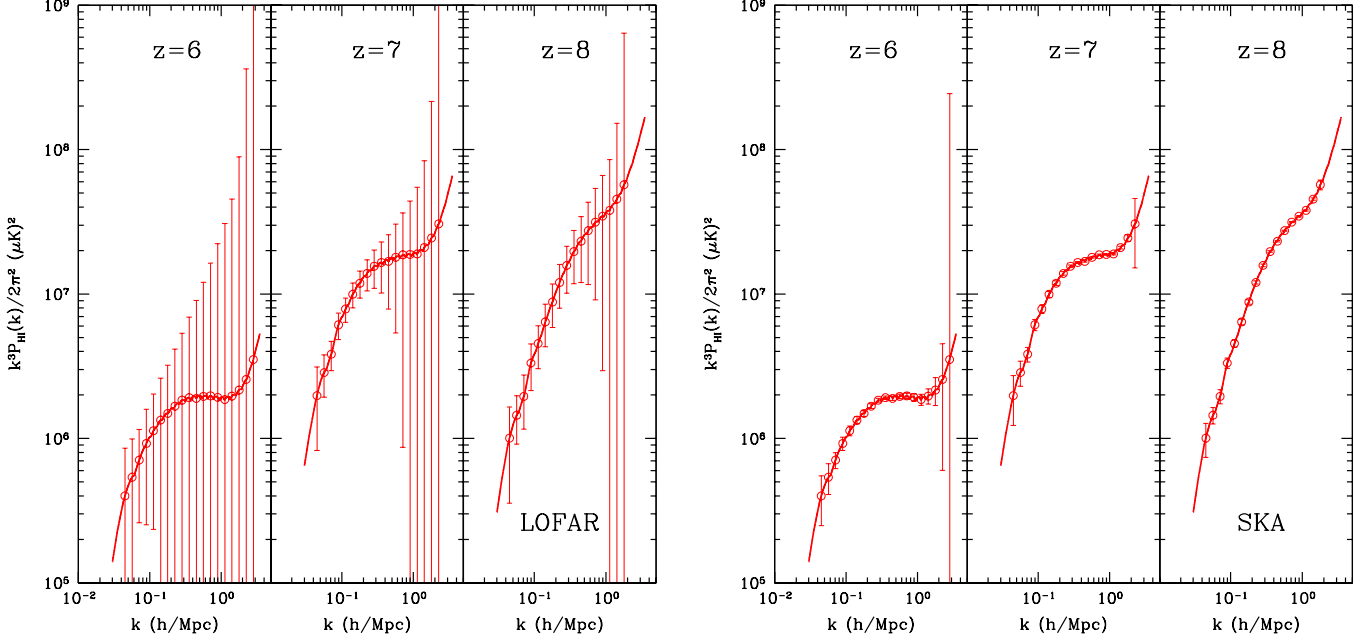
FIG. 11.— The power spectrum of 21-cm emission at z=6, z=7 and z=8. The error bars in the left panel are estimated with a setup similar to LOFAR while the ones in the right panel are from a setup similar to SKA.
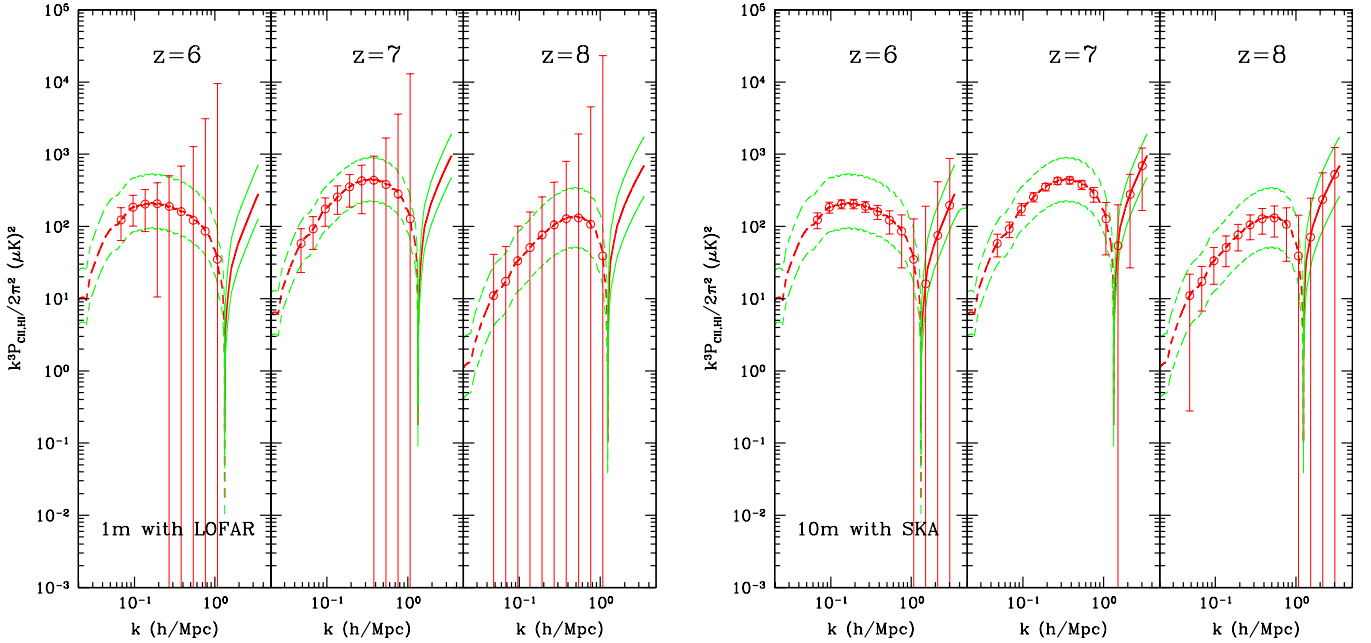

FIG. 12.— The cross power spectrum of the CII and the 21-cm emission line at $z = 6$, $z = 7$ and $z = 8$. The red dashed lines denote the negative correlations while the red solid lines denote positive correlations. The 1σ errors are also shown in thin red lines. Here we just consider the 21-cm signal from the IGM, since the 21-cm signal from neutral gas in galaxies is about 10^{-4} of the IGM signal (Gong et al. 2011). The error bars in the left panel are estimated using the (sub-) milimeter survey with a 1 m aperture for CII line with a setup similar to LOFAR for 21-cm measurements, while 10 m aperture for CII line with a setup similar to SKA for 21-cm measurements in the right panel.

cross-power spectrum, which to linear order is given by

$$P_{\mathrm{CII,HI}}(z,k) \propto 4/3(1 - \bar{x}_{\mathrm{i}})P_{\delta\delta} - \bar{x}_{\mathrm{i}}P_{\delta_x\delta}, \qquad (19)$$

where $\bar{x}_{\mathrm{i}}$ is the average ionization fraction and $P_{\delta_x\delta}$ is the cross power spectrum of the ionized fraction and the dark matter. The transition scale is related to the typical

ionized bubble size. To show the cross-correlation illustratively, we also plot the cross-correlation coefficient at $z = 6$, $z = 7$ and $z = 8$ in Fig. 13, which is estimated by $r_{\mathrm{CII,HI}}(k) = P_{\mathrm{CII,HI}}(k)/\sqrt{P_{\mathrm{CII}}(k)P_{\mathrm{HI}}(k)}$.
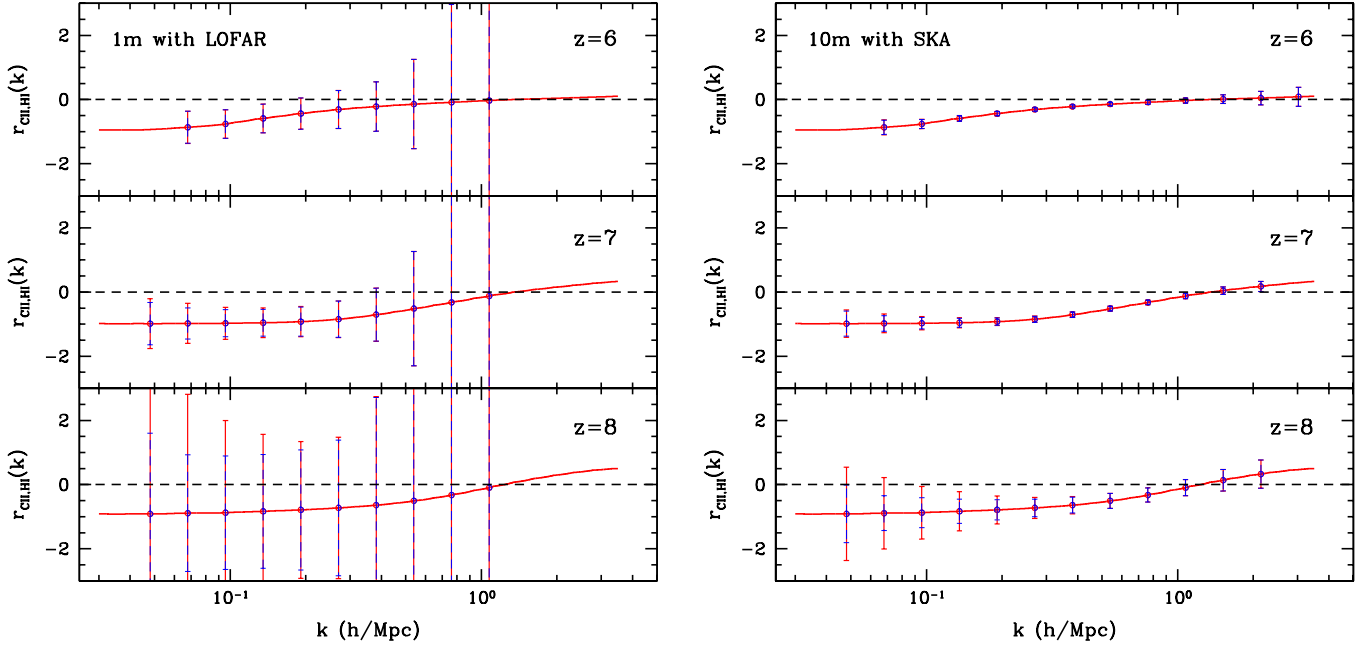
Fig. 13.— The cross-correlation coefficient of the CII and 21-cm emission for 1m and 10m aperture at $z = 6$, $z = 7$ and $z = 8$. The error bars of r are also shown (red solid), and the blue dashed ones are the contribution from the 21-cm emission with the LOFAR (left panel), and with the SKA (right panel). We find the 21-cm noise dominates the errors at z=6 and 7.

7. OUTLINE OF A CII INTENSITY MAPPING EXPERIMENT

We now discuss the requirements on an instrument designed to measure the CII line intensity variations and the power spectrum at $z > 6$. Here we provide a sketch of a possible instrument design including calculated noise requirements based on current technology; a detailed design study will be left to future work as our concept is further developed.

An experiment designed to statistically measure the CII transition at high redshift requires a combination of a large survey area and low spectral resolution; because of this, the use of an interferometer array such as the one suggested in Gong et al. (2011) for CO seems impractical. Instead we opt for a single aperture scanning experiment employing a diffraction grating and bolometer array in order to provide large throughput.

For proper sampling of the CII signal on cosmological scales and cross-correlation with 21-cm experiments, we would require at minimum a survey area of 16 deg^2 and a free spectral range (FSR) of 20 GHz. At a redshift of $z = 7$, a box 4 degrees on a side and 20 GHz deep corresponds to a rectangular box with a comoving angular width of 443 Mpc/h and a depth along the line of sight of 175 Mpc/h. However, since larger FSRs are easily achieved with diffraction grating architectures and would allow for better measurement of the reionization signal and separation of its foregrounds, the instrumental concept presented here covers the 220 GHz atmospheric window with an FSR of 125 GHz. Concretely, covering from 185 to 310 GHz with a spectral resolution of 0.4 GHz allows measurement of CII in the range $5.1 \leq z \leq 9.3$ with a smallest redshift interval Δz of 0.01.

The integration time per beam on the sky required to survey a fixed area depends on a number of parameters including the size of the aperture, the number of independent spatial pixels in the spectrometer, and the bandwidth of each spectral element. Changing the survey area or bandwidth will affect the minimum k values probed in the 3-d power spectrum as well as the number of modes used in the error calculation. To generate concrete examples in this discussion, we concentrate on calculating the CII power spectrum at $z = 6$, 7 and 8 and assume that we will make use of 20 GHz effective bandwidths at frequencies centered at these redshifts; such effective bands are readily achieved by summing neighbouring high resolution spectral bins. At $z = 7$, for example, a 20 GHz bandwidth corresponds to a $\Delta z = 0.62$. Averaging over a larger spectral window to reduce noise will make the cosmological evolution along the observational window non-negligible.

To understand the effect of spatial resolution on this measurement we consider three possible primary aperture sizes of 1, 3 and 10 m; the resulting instrumental parameters are listed in Table 1. These apertures correspond yield beams of 4.4, 1.5, and 0.4 arcmin and comoving spatial resolutions of 8.3, 2.8, 0.8 Mpc/h at an observing frequency of 238 GHz ($z = 7$), respectively. These apertures probe the linear scales ($k < 1.0$ h/Mpc) and are well matched to 21-cm experiments. In this experimental setup light from the aperture is coupled to a imaging grating dispersive element illuminating a focal plane of bolometers, similar to the Z-Spec spectrometer but with an imaging axis (Naylor et al. 2003; Bradford et al. 2009).

We assume a fixed spectral resolution of ~ 500 km/s ($= 0.4$ GHz as discussed above) in each of the three cases giving a spatial resolution of 3.5 Mpc/h and a maximum k mode of $k \approx 0.91$ h/Mpc. Current technology can allow fabrication of $\sim 20,000$ bolometers in a single focal plane; for the instrument concept we freeze the number of detectors at this value. The spectrometric sensitivity

TABLE 1
EXPERIMENTAL PARAMETERS FOR A POSSIBLE CII MAPPING INSTRUMENT.

Aperture diameter (m)	1	3	10
Survey Area (deg^2)	16	16	16
Total integration time (hours)	4000	4000	4000
Free spectral range (GHz)	$185-310$	$185-310$	$185-310$
Freq. resolution (GHz)	0.4	0.4	0.4
Number of bolometers	20,000	20,000	20,000
Number of spectral channels	312	312	312
Number of spatial pixels	64	64	64
Beam size[a] (FWHM, arcmin)	4.4	1.5	0.4
Beams per survey area[a]	2.6×10^3	2.3×10^4	2.6×10^5
$\sigma_{\rm pix}$: Noise per detector sensitivity[a] (Jy$\sqrt{s}$/sr)	2.5×10^6	2.5×10^6	2.5×10^6
$T_{\rm pix}$: Integration time per beam[a] (hours)	100	11	1.0
$z = 6$ $V_{\rm pix}$ (Mpc/h)^3	216.5	23.7	2.1
$z = 7$ $V_{\rm pix}$ (Mpc/h)^3	332.4	36.8	3.3
$z = 8$ $V_{\rm pix}$ (Mpc/h)^3	480.0	53.1	4.7
$z = 6$ $P_N^{\rm CII}$ (Jy/sr)^2 (Mpc/h)^3	3.7×10^9	3.7×10^9	3.6×10^9
$z = 7$ $P_N^{\rm CII}$ (Jy/sr)^2 (Mpc/h)^3	5.7×10^9	5.8×10^9	5.7×10^9
$z = 8$ $P_N^{\rm CII}$ (Jy/sr)^2 (Mpc/h)^3	8.3×10^9	8.4×10^9	8.1×10^9

[a] values computed at 238 GHz, corresponding to CII at $z = 7$.

of the grating spectrometer design is estimated using a model of the instrument which includes loading from the CMB, atmosphere and instrument contributions assuming realistic temperatures and emissivities for each.

The noise equivalent power of the background ($NEP_{\rm BG}$) is computed as the quadrature sum of contributions from Phonon, Johnson, Shot and Bose noise terms using these loadings and estimates of realistic instrument parameters from existing experiments (e.g. Brevik et al. 2010). Similarly, the total $NEP_{\rm tot}$ of the instrument is the square root of the quadrature sum of $NEP_{\rm BG}$ and a detector with $NEP_{\rm Det} = 1 \times 10^{-18}$ W HZ$^{-1/2}$, a value readily achieved using current detector technology. $NEP_{\rm tot}$ does not depend on the size of the telescope aperture; to convert this to the corresponding noise equivalent flux density (NEFD) in Jy s$^{1/2}$ we use

$$\mathrm{NEFD} = \frac{\mathrm{NEP}_{\rm tot}}{\eta_{\rm sys} A \sqrt{2\Delta\nu} \exp(-\eta_{\rm sky})} \qquad (20)$$

where A is the area of the telescope aperture. As an example, for a 3 m aperture at 238 GHz these parameters result in an estimated NEFD of 0.42 Jy s$^{1/2}$ per pixel per spectral resolution element. This NEFD can then be converted to the units of Jy s$^{1/2}$/sr used in Table 1 by multiplication by the solid angle of the telescope response. For observations corresponding to $z = 7$, this results in a noise per pixel of 2.5×10^6 Jy s$^{1/2}$/sr.

The statistical detection shown in figure 8 using the instrumental parameters listed in Table 1 can be obtained by noting that the error on each of the binned power spectrum measurements is $\Delta P = (P_N^{\rm CII} + P_{\rm CII})/\sqrt{N_m}$, where $P_{\rm CII}$ is the CII power spectrum, including shot-noise, and N_m the number of modes contributing to each bin. The noise power spectrum $P_N^{\rm CII}$ for CII observations using the spectrometer as described in above can be written as

$$P_N^{\rm CII} = V_{\rm pix} \frac{\sigma_{\rm pix}^2}{T_{\rm pix}} . \qquad (21)$$

The values for the experimental setup is tabulated in Table 1. These noise power spectra are also shown for the 1 and 10 meter aperture in Fig. 8. The proposed

CII experiments involve three different apertures at 1, 3, and 10 m, but all three options make use of the same spectrometer with a total $\sim$ 20,000 bolometers that make up 64 individual pixels on the sky.

Taking into account these number of modes allowed by the observational window, the noise parameters and with an integration time of 4000 hours, the CII power spectrum at $z = 6$ is detected with a signal-to-noise ratio, S/N $= \sqrt{\sum_{\rm bins} \left(\frac{P(k)}{\Delta P(k)} \right)^2}$, of 12, 15, and 18 for 1, 3, and 10 m aperture cases, respectively. The corresponding values for $z = 7$ are 2, 3, and 5 respectively, while at $z = 8$ the signal-to-noise ratio values are less than 1 for all three options.

For the cross-correlation with 21-cm data, we assume that observations will be conducted in overlapping areas on the sky by both the CII and the 21-cm experiment. This is a necessary feature of cross-correlation study leading to some coordination between two experiments. We reduce both data sets to a common, and a lower resolution cube in frequency and count the total number of common modes contributing to a given bin in k space using the same method for noise calculation as in Gong et al. (2011). The error in a given k bin can be written as $\sqrt{(P_{\rm CII,H}^2 + P_{\rm CII}P_{\rm H})/(2N_m)}$, where N_m is the number of modes falling in that bin.

When describing the 21-cm observations we assume sensitivities similar to LOFAR and SKA with parameters following Gong et al. (2011) with $A_{\rm tot} = 7 \times 10^4$ m^2 and $T_{\rm sys} = 490$K at 150 MHz, bandwidth of 12 MHz, and resolution of 0.25 MHz (see Table 2 for SKA parameters). The noise power spectrum amplitude $P_N^{21-\rm cm}$ is a constant and takes the form as

$$P_N^{21-\rm cm}(k,\theta) = D_A^2 y(z) \frac{\lambda^4 T_{sys}^2}{A_{\rm tot}^2 t_0 n \left(D_A k \sin(\theta)/2\pi \right)}, \qquad (22)$$

where D_A is the comoving angular diameter distance, $A_{\rm tot}$ is the collecting area for one element of the interferometer, t_0 is the total integration time and the function $n()$ captures the baseline density distribution on the plane perpendicular to the line of sight, assuming it is al-

Instrument	LOFAR	SKA
FoV (deg^2)	25	25
Bandwidth (MHz)	12	12
Freq. resolution (MHz)	0.25	0.25
System temperature (K)	449	369
maximum baseline (m)	2000	2000
Total integration time (hours)	1000	4000
total collecting area at 150 MHz (m^2)	7.0×10^4	1.4×10^6
$z=6$ $P_N^{21-\mathrm{cm}}$ [K^2 (Mpc/h)^3]	1.9×10^{-1}	1.0×10^{-3}
$z=7$ $P_N^{21-\mathrm{cm}}$ [K^2 (Mpc/h)^3]	2.5×10^{-1}	1.5×10^{-3}
$z=8$ $P_N^{21-\mathrm{cm}}$ [K^2 (Mpc/h)^3]	3.4×10^{-1}	2.3×10^{-3}

ready rotationally invariant (k is the moduli of the wave mode $\mathbf{k}$ and θ is the angle between $\mathbf{k}$ and the line of sight) (Santos et al. 2011; Gong et al. 2011). The cross-correlation is detected with a signal-to-noise ratio of 4 to 5 at $z=6$ and 5 to 8 at $z=7$ when any of the three CII options is combined with LOFAR. There is a factor of a 3 to 4 improvement when combined with SKA leading to signal-to-noise ratios of 12, 13 and 14 for the $z=6$ cross-correlation with 1, 3, and 10 m options, respectively. At $z=7$, the signal-to-noise ratios are 12, 15, and 20, while at $z=8$ they are 4, 5 and 7, respectively. While the CII power spectrum cannot be detected at $z=8$ using any of the three options in Table 1, the cross-correlations can be detected when one of the proposed CII experiments is combined with SKA.

The cross-correlation coefficient between CII and 21-cm (Fig. 12) shows a transition from negative to positive values due to the size of the ionized bubbles surrounding galaxies during reionization (Eq. 19). The transition scale from positive to negative captures both the size of the typical ionized bubbles and the mean value of the ionization fraction $\bar{x}_i$. The observational measurement of this negative to positive transition is challenging for a first-generation CII experiment involving 1 or 3 m aperture combined with a first-generation 21-cm experiment like LOFAR, but is likely to be feasible with an improved CII experiment combined with SKA.

8. CONCLUSION AND DISCUSSION

In this paper, we have estimated the mean intensity and the spatial intensity power spectrum of the CII emission from galaxies at $z>6$. We first calculated the CII intensity analytically for both the ISM of galaxies and the diffuse IGM and showed that the CII emission from dense gas in the ISM of galaxies is much stronger than that from the IGM. Then, to check the analytical calculation, we used the hot gas or the hot+warm gas from a

simulation to find the CII mass in a halo, and further calculated the CII number density and intensity. We found that the two methods are in good agreement especially at high redshifts we are interested in. Next, we computed the CII clustering power spectrum assuming the CII luminosity is proportional to the CII mass, $L_{\mathrm{CII}} \sim M_{\mathrm{CII}}$. We compared our CII power spectrum with that derived from the L_{CII}-$L_{\mathrm{CO}(1-0)}$ relation, and found that they are consistent in the 1σ level. We also explored the contamination of the CII emission by the CO lines at lower redshift, and found the contamination can lead to 2% and 30% enhancement of the CII power spectrum at $z=7$ and $z=8$.

To reduce the foreground contamination and to improve our scientific understanding of reionization we propose here a cross-correlation study between the CII and 21-cm emission in the overlapping redshift ranges and the same part of the sky. The cross-correlation exists since they both trace the same matter distribution. At large scales the correlation is due to ionized bubbles surrounding CII bright galaxies while at smaller scales both CII galaxies and ionized bubbles trace the underlying density field. We have outlined 3 potential CII experiments using 1, 3 and 10 m aperture telescope outfitted with a bolometer array spectrometer with 64 independent spectral pixels. A 1 or 3 meter aperture CII experiment is matched to a first generation 21-cm experiment such as LOFAR while an improved CII experiment can be optimized to match a second generation 21-cm experiment like SKA. We find that the overall ability to extract details on reionization requires a careful coordination and an optimization of both CII and 21-cm experiments. We have not discussed the issues related to foregrounds, including AGN-dominated radio point sources that dominate the low-frequency observations and dusty galaxies that dominate the high-frequency CII observations and Galactic foregrounds such as dust and synchrotron. In future papers we will return to these topics and also expand our discussion related to the instrumental concept as we improve the existing outline to an actual design.

REFERENCES

Aguirre, A. & Schaye, J. 2005, pgqa. conf. 289
Arnett, D. 1996, Supernovae and Nucleosynthesis, Princeton, New Jersey: Princeton University Press
Basu, K., Hernandez-Monteagudo, C. & Sunyaev, R., A. 2004, A&A., 416, 447
Benford, D. J., Hunter, T. R., & Phillips, T. G. 1998, International Journal of Infrared and Millimeter Waves, 19, 7.
Bock, J. J., Hristov, V. V., Kawada, M. et al. 1993, ApJ, 410, L115
Boselli, A., Gavazzi, G., Lequeux, J. & Pierini, D. 2002, A&A, 358, 454
Bouwens, R. J. et al. 2008, ApJ, 686, 230

Bradford, C. M., et al. 2009, ApJ, 705, 112
Breuck, C. D., et al. 2011, arXiv:1104.5250
Brevik, J. A., et al. 2010, Proc. SPIE, 7741, 41
Carilli, C. L. 2011, ApJ, 730, L30
Crawford, M. K., Genzel, R., Townes, C. H. & Watson, D. M. 1985, ApJ, 291, 755
Dalgarno, A. & McCray, R. 1972, ARA&A, 10, 375
Datta, A, Bowman, J. D. & Carilli, C. L. 2010, ApJ, 724, 526
De Looze, I., Baes, M., Bendo, G. J., Cortese, L., Fritz, J. 2011, MNRAS in press, arXiv.org:1106.1643
De Lucia, G. & Blaizot, J. 2007, MNRAS, 375, 2
Field, G. B. 1958, Proc. I. R. E., 46, 240

Fukugita, M. & Kawasaki, M. 1994, MNRAS, 269, 563

Furlanetto, S., Peng Oh, S. & Briggs, F. 2006, Phys. Rept. 433, 181

Giallongo, E., Cristiani, S., D'Odorico, S., Fontana, A. & Savaglio, S. 1997, seim. proc. 127

Gong, Y., Cooray, A., Silva, M. B., Santos, M. G. & Lubin, P. 2011, ApJ, 728, L46

Haiman, Z., Abel, T. & Rees, M. 2000, ApJ, 534, 11

Hernandez-Monteagudo, C., Haiman, Z., Jimenez, R. & Verde, L. 2006, arXiv:0612363

Hernandez-Monteagudo, C., Haiman, Z., Verde, L. & Jimenez, R. 2008, ApJ, 672, 33

Keenan, F. P., Lennon, D. J., Johnson, C. T. & Kingston, A. E. 1986, MNRAS, 220, 571

Kistler, M. D., et al. 2009, ApJ, 705, L104

Komatsu, E., et al. 2011, ApJS, 192, 18

Kramer, R. H., Haiman, Z. & Madau, P. 2010, arXiv:1007.3581

Kulkarni, V. P., Fall, S., M., Lauroesch, J. T., York, D. G. & Welty, D. E. 2005, ApJ, 618, 68

Lehner, N., Wakker, B. P. & Savage, B. D. 2004, ApJ, 615, 767

Lidz, A. et al. 2011, arXiv.org:1104.4800

Malhotra, S., et al. 2001, ApJ, 561, 766

Nagamine, K., Wolfe, A. M. & Hernquist, L. 2006, ApJ, 647, 60

Naylor, B. J., et al. 2003, in Society of Photo-Optical Instrumentation Engineers (SPIE) Conference, Vol. 4855, Society of Photo-Optical Instrumentation Engineers (SPIE) Conference Series, ed. T. G. Phillips & J. Zmuidzinas, 239248

Obreschkow, D., Croton, D., De Lucia, G., Khochfar, S. & Rawlings, S. 2009a, ApJ, 698, 1467

Obreschkow, D., Klockner, H.-R., Heywood, I., Levrier, F. & Rawlings, S. 2009b, ApJ, 703, 1890

Osterbrock, D. E. 1989, Astrophysics of Gaseous Nebulae and Active Galactic Nuclei (Mill Valley: Univ. Science Books)

Pei, Y. C., & Fall, S. M. 1995, ApJ, 454, 69

Pei, Y. C., Fall, S. M., & Hauser, M. G. 1999, ApJ, 522, 604

Santos, M. G., et al. 2008, ApJ, 689, 1

Santos, M. G., Ferramacho, L., Silva, M. B., Amblard, A. & Cooray, A. 2010, MNRAS, 406, 2421

Santos, M. G., Silva, M. B., Pritchard, J. R., Cen, R. & Cooray, A. 2011, A&A, 527, A93

Savaglio, S. 1997, seim. proc. 73

Sheth, R. K. & Tormen, G. 1999, MNRAS, 308, 119

Smith, R. E., et al. 2003, MNRAS, 341, 1311

Spitzer, L. J. 1978, Physical Processes in the Interstellar Medium (New York: Wiley)

Springel, V., et al. 2005, Nature, 435, 629

Stacey, G. J., Geis, N., Genzel, R., Lugten, J. B., Poglitsch, A., Sternberg, A. & Townes, C. H. 1991, ApJ, 373, 423

Stacey, G. J., et al. 2010, ApJ, 724, 957

Suginohara, M., Suginohara, T. & Spergel, N., 1999, ApJ, 512, 547

Tayal, S. S. 2008, A&A., 486, 629

Tielens, A. G. G. M. & Hollenbach, D. 1985, ApJ, 291,722

Visbal, E. & Loeb, A. 2010, JCAP, 11, 016

Walter, F., Riechers, D., Cox, P., Neri, R., Carilli, C., Bertoldi, F., Weiss, A. & Maiolino, R. 2009, Nature, 457, 699

Wolfire, M. G., et al. 1995, ApJ, 443, 152

Wouthuysen, S. A. 1952, AJ, 57, 31

Wright, E. L., et al. 1991, ApJ, 381, 200